Theoretical and experimental investigation of the equations of state and phase stabilities of MgS and CaS

1996 J. Phys.: Condens. Matter 8 8251

(http://iopscience.iop.org/0953-8984/8/43/018)

J. Phys.: Condens. Matter **8** (1996) 8251–8265. Printed in the UK

Theoretical and experimental investigation of the equations of state and phase stabilities of MgS and CaS

Shirley Ekbundit†, Andrew Chizmeshya†‡, Randall LaViolette‡ and George H Wolf†

† Department of Chemistry, Arizona State University, Tempe, AZ 85287-1604, USA
‡ Idaho National Engineering Laboratory, EG&G Idaho, PO Box 1625, Idaho Falls, ID 83415-2208, USA

Received 7 December 1995, in final form 16 May 1996

Abstract. The equations of state and phase stabilities of MgS and CaS are investigated via non-empirical theoretical calculations using three different electron-gas models: the self-consistent ion breathing (SCIB), the variationally induced breathing (VIB) and the potential-induced breathing (PIB) models. We apply these models on an equal footing using Kohn–Sham ionic densities and identical interaction density functionals. The calculated equations of state are compared to the compression curves of MgS at pressures up to 54 GPa and of CaS at pressures up to 52 GPa. The accuracies of the three electron-gas models in reproducing the equations of state of both compounds are generally comparable to those previously achieved for the binary oxide and halide systems. We also investigate the phase stabilities of MgS and CaS in CsCl (B2), wurtzite (B4) and zincblende (B3) structures. Our calculations accurately determine the B1–B2 phase transition for CaS. In the case of MgS, the transition pressure is much higher than that of the current experimental measurement ranges. In addition, the models predict that the B4 phases of MgS and CaS can be stabilized under moderate tensions. This result is consistent with experimental observation of epitaxially stabilized MgS wurtzite films.

1. Introduction

The high-pressure behaviours displayed by closed-shell alkali halides and alkaline-earth chalcogenides have long been a proving ground in theoretical condensed matter physics. First-principles calculations have been very successful in predicting the phase stability, metallization transitions and high-pressure equations of state of a number of alkali metal halides and alkaline-earth chalcogenides [1–7]. However, simpler and more efficient, non-empirical models have also been found to be reasonably reliable in predicting the equations of state and phase stabilities of binary alkali halide and alkaline-earth oxide compounds. In this latter regard, there has been a flurry of interest in Gordon–Kim-type schemes in which the total crystal charge density is approximated by the overlap of spherical closed-shell ions and the atomic interactions are estimated using density functional theory [8]. The most reliable of these electron-gas methods are those that incorporate relaxation of the component ion charge densities and thus include, at least to leading order, volume-dependent many-body effects [9–16]. Although the Gordon–Kim-based methods have been well tested for binary oxide and halide closed-shell systems, very little has yet been done concerning the application of approximate electron-gas models to sulphide systems.

To evaluate and compare the reliability of such models, we have calculated the equations of state (EOS) and high-pressure phase stabilities of MgS and CaS using three popular

0953-8984/96/438251+15$19.50

variants. In all three of these, the S^{2-} charge density is allowed to deform spherically in response to its crystal environment. In the potential-induced breathing (PIB) [9, 10, 14] and variationally induced breathing (VIB) models [11, 16], the crystal potential is represented by that of a Watson sphere [18]. The only difference between these two schemes is that, in PIB, the parameters defining the Watson potential are solely determined by the ion's Coulomb site potential whereas in VIB the Watson potential parameters are obtained through a variational procedure. In the more elaborate self-consistent ion breathing (SCIB) model [12, 13, 30], the effective crystal potential is not constrained to a Watson-sphere form but is given by a self-consistent spherically averaged crystal potential which incorporates both the Coulomb and the overlap exchange and kinetic energy terms. In order to determine the relative accuracy among these models, we compare the calculated EOSs and the bulk moduli with experimental values.

At ambient pressure, both MgS and CaS crystallize in the rock-salt (B1) structure. Both compounds are expected to undergo a B1–B2 structural transformation at high pressure, following a general trend found in most alkaline-earth chalcogenide series. The only high-pressure study for MgS was conducted by Peiris *et al* [17] up to 54 GPa. Within the pressure range of those experiments, no phase transition was observed. Conversely, several studies have been performed on CaS. The earliest high-pressure study was conducted by Bridgman [28] up to 5 GPa. A later study by Perez-Albuerne and Drickamer [27] extended the highest pressure to 35 GPa. These studies found that the B1 phase remains stable up to their highest pressure; however, the EOS obtained by Perez-Albuerne and Drickamer [27] exhibits an anomalously large decrease in compressibility at high pressure such that they cannot fit this data set to the Born–Mayer model. A subsequent theoretical study on CaS by Schlosser and Ferrante [26] also indicated difficulty in fitting this data set with their model beyond 23 GPa. For this reason we have re-measured the EOS of CaS up to 39 GPa using energy dispersive x-ray diffraction. In contrast to previous results, no evidence for anomalous compressibility was observed at high pressure and the B1 phase remains stable up to the highest pressure of the experiment. During the preparation of this paper, the experiment of Luo *et al* [42] emerged in the literature, in which the EOS of CaS was measured up to 52 GPa and the B1–B2 phase transition was observed near 40 GPa. Slight differences in the measured EOS are observed among the data sets; this may be due to the degree of hydrostaticity since no medium was used by Luo *et al* [42] whereas both methanol:ethanol and argon were used as pressure media in our study. In the following section we compare our theoretical model calculations with our own data and those of Luo *et al* [42].

We find that the accuracy of the three electron-gas models in reproducing the measured EOSs of MgS and CaS is generally comparable to those previously achieved for binary oxide and halide systems. Moreover, similarly to that which we have found in oxide and nitride systems (in preparation), the best overall results are achieved in those models when a non-empirical, self-consistent scaling functional for the kinetic energy interaction is used.

2. Experimental and data analysis

2.1. Experimental procedures

Polycrystalline CaS with a stated purity of 99.9%, was compacted into small discs about 15 μm thick and loaded into the sample chamber of a Mao–Bell-type diamond anvil cell. Two diffraction experiments were performed. In the first (run 1), a 4:1 methanol:ethanol pressure transmitting fluid was used and the maximum pressure was limited to 10 GPa (slightly below the solidification point of this medium) to ensure complete hydrostaticity.

The pressure in this cell was measured using the ruby fluorescence method [19]. The second compression experiment (run 2) was performed under quasi-hydrostatic conditions using argon both as a pressure medium and as an internal pressure calibrant. The 111 and 220 argon diffraction peaks were used to determine the argon volume. The corresponding pressure was determined from the argon EOS which was obtained from fitting all currently available high-pressure argon data [20–24] to the third-order Birch–Murnaghan equation of state using $V_0 = 22.557$ cm^3 mol^{-1}, $K_0 = 4.83$ GPa and $K_0' = 5.33$.

The energy dispersive x-ray diffraction data were obtained at Brookhaven National Light Source on beam line X17C. In order to minimize the effects of pressure gradients, the incident x-ray beam was collimated at a 25 μm $\times$ 25 μm spot and diffraction data from the CaS sample and the argon pressure calibrant were obtained together. The diffracted radiation was collected using a solid-state germanium detector fixed at a 2θ angle of $13.012^\circ(\pm 0.005^\circ)$. The high-pressure unit cell volumes of the B1 phase were determined using 5–7 diffraction lines. The ambient-pressure volume (V_0) of CaS was obtained on an angle-dispersive Rigaku diffractometer. From a Rietveld fit to the powder diffraction data, V_0 was determined to be 46.191 ± 0.004 Å^3 which agrees with literature value (International Centre for Diffraction Data) to within 0.04%.

Table 1. Compression data of CaS.

P (GPa)	V (Å^3)	Number of diffraction peaks used in determining the volume	V_{Ar} (Å^3/atom)
0	46.19 ± 0.02		
1.22 ± 0.20	45.37 ± 0.10	7	
2.26 ± 0.20	44.15 ± 0.12	7	
3.26 ± 0.20	43.62 ± 0.12	6, 6[a]	
4.70 ± 0.20	42.71 ± 0.02	6	
5.93 ± 0.20	42.14 ± 0.17	5, 6[a]	
6.94 ± 0.20	41.84 ± 0.27	6, 3[a]	
8.12 ± 0.20	41.19 ± 0.09	6, 3[a]	
9.19 ± 0.20	40.64 ± 0.12	6, 3[a]	
10.33 ± 0.75[b]	40.18 ± 0.15	6	22.16 ± 0.36
16.13 ± 0.83[b]	38.32 ± 0.24	5	20.17 ± 0.25
19.14 ± 0.85[b]	37.09 ± 0.15	6	19.25 ± 0.21
25.72 ± 1.47[b]	35.50 ± 0.17	6	17.91 ± 0.26
31.13 ± 1.19[b]	34.33 ± 0.11	6	17.08 ± 0.17
35.91 ± 1.33[b]	33.44 ± 0.17	6	16.48 ± 0.16
39.23 ± 1.56[b]	32.79 ± 0.14	6	16.10 ± 0.17

[a] Diffraction peaks taken from two independent spectra at the same pressure.
[b] Pressure error represents propagated error in V_{Argon}.

2.2. Experimental results and discussion

Representative energy dispersive x-ray diffraction patterns of CaS, given for runs 1 and 2 at several different pressures, are shown in figure 1. The x-ray patterns agree well with undistorted B1 structure up to 39 GPa. The pressure–volume data are shown in figure 2 and summarized in table 1. Our low-pressure data are reasonably consistent with earlier measurements [27, 28, 42]. However, above 20 GPa the data of Perez-Albuerne and Drickamer [27] systematically show a smaller degree of compression than do our data. A similar discrepancy in CaO above 20 GPa was also noted by Richet *et al* [29] in a

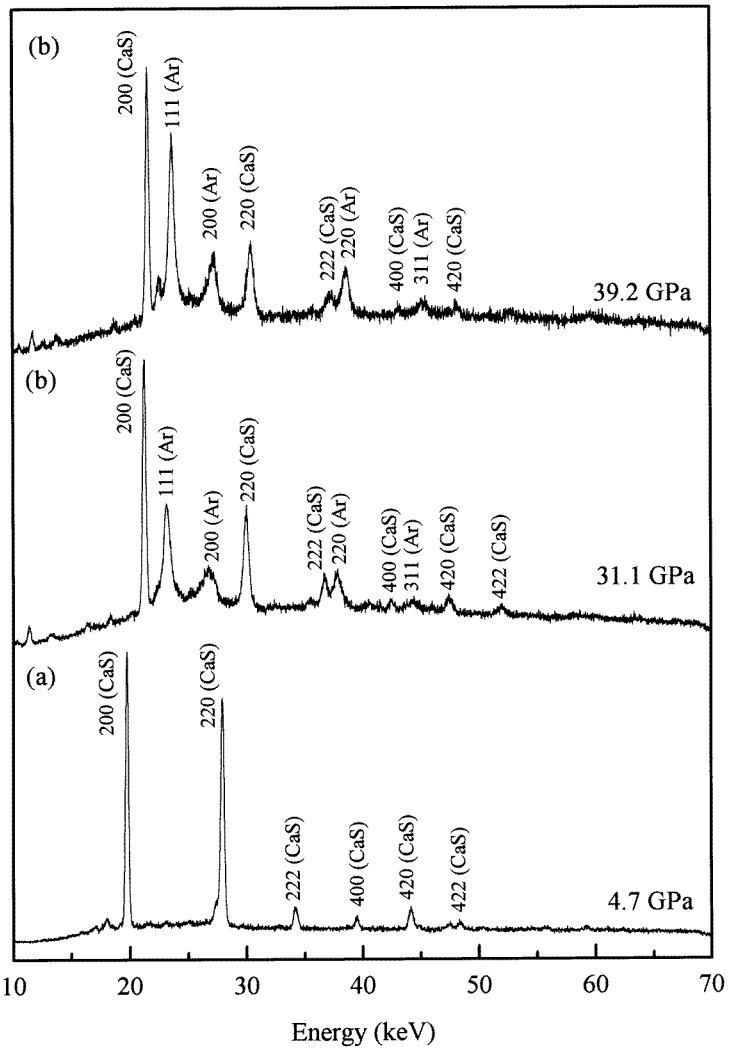

Figure 1. *In situ* EDXD spectra of CaS for (a) run 1 at 4.7 GPa (hydrostatic) and (b) run 2 at 31.1 and 39.2 GPa (quasi-hydrostatic). In run 2, diffraction peaks due to the argon pressure medium are also observed.

comparison of their high-pressure data with the earlier CaO data of Perez-Albuerne and Drickamer [27]. The EOS obtained by Luo *et al* [42] starts to deviate slightly from ours as low as 10 GPa. The greater scatter of their data in comparison to ours may be due to a greater degree of non-hydrostaticity. Near 40 GPa, Luo *et al* [42] observed a signature of the B2 phase of CaS which remains visible to their highest pressure of 52 GPa.

The compression data were analysed using both the Birch–Murnaghan [25] and the universal [41] EOSs. The Birch–Murnaghan EOS is based on an Eulerian strain expansion of the Helmholtz free energy. If this energy expansion is performed to third-order in the strain, f, then the pressure, P, can be expressed as

$$P = 3K_0 f(1+2f)^{5/2}[1 - \tfrac{3}{2}(4 - K_0')f]. \tag{1}$$

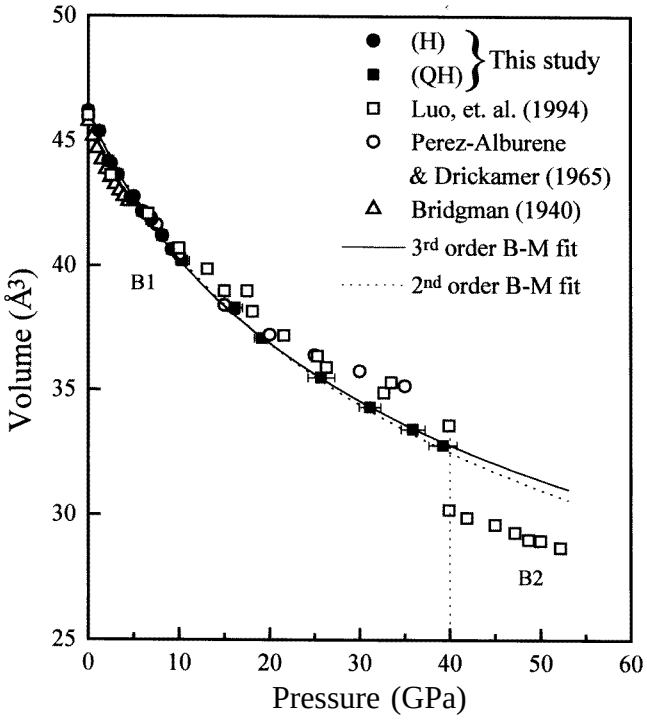

Figure 2. Compression data of the B1 and B2 phases of CaS. Filled circles and filled squares represent the hydrostatic (H) and quasi-hydrostatic (QH) data taken in this study. Data for CaS from Luo *et al* [42] (open squares), Perez-Albuerne and Drickamer [27] (open circles) and Bridgman [28] (triangles) are also shown. The full and broken lines represent the respectively third-order and second-order Birch–Murnaghan fits to the data. The universal EOSs and the third-order Birch–Murnaghan EOSs are indistinguishable.

Here K_0 and K_0' are the isothermal bulk modulus and its pressure derivative at ambient pressure, and the Eulerian strain measure is defined by $f = \frac{1}{2}[(V_0/V)^{2/3} - 1]$. In the expression for f, V is the volume of the sample and V_0 is the reference volume at ambient pressure. The third-order Birch–Murnaghan EOS can be expressed as a linear relation between a normalized stress, F, defined as $F \equiv P/[3f(1+2f)^{5/2}]$, and the strain, f. In the linear F versus f equation, given by

$$F(f) = K_0[1 - \tfrac{3}{2}(4 - K_0')f] \tag{2}$$

the intercept is K_0 and the slope is related to K_0'. The F versus f data for CaS is shown in figure 3. The different trends observed in the F versus f plot above and below $f = 0.03$ could be due to the different hydrostaticity conditions of the methanol:ethanol and argon pressure media. The line plotted in figure 3 is an error-weighted linear least-squares fit to the F versus f data. Only the error in F is used in the least-squares weighting scheme (see [40]). From the fit, we obtain values of $K_0 = 51.9 \pm 1.2$ GPa and $K_0' = 4.7 \pm 0.2$. A fit to the data using a second-order Birch–Murnaghan EOS ($K_0' = 4.0$) yields a value of 56.4 ± 2.2 GPa for K_0. In comparison, Luo *et al* [42] obtained $K_0 = 64$ GPa with $K_0' = 4.2$.

The universal EOS [41] has been found to describe the pressure–volume relationships of a broad class of materials accurately. This EOS is based on a scaled relationship between

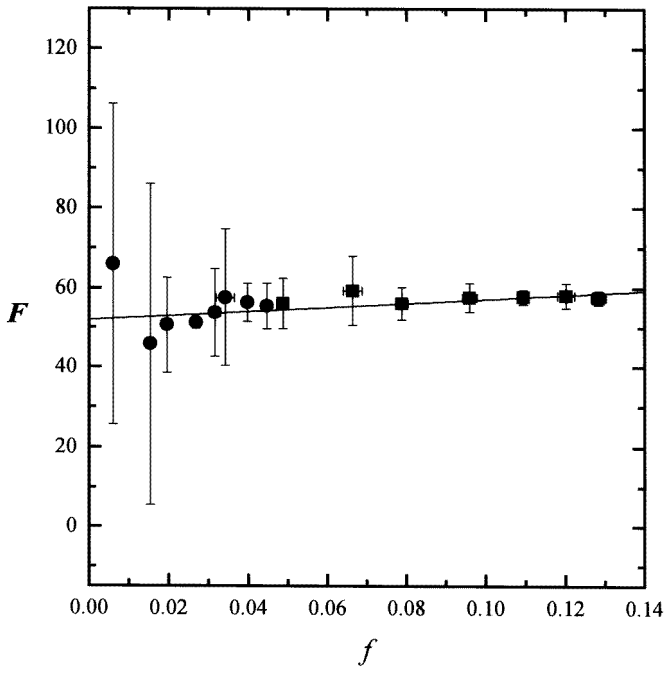

Figure 3. A Birch–Murnaghan F versus f plot for the CaS data. The filled circles represent hydrostatic data from run 1 using methanol:ethanol as the pressure medium and the filled squares represent the quasi-hydrostatic data obtained from run 2 using the argon pressure medium. The full line is a third-order Birch–Murnaghan fit to the data.

binding energy and interatomic separation. The analytical expression used for the universal equation of state is given by the form

$$P = \frac{3K_0(1-X)}{X^2}\exp\left[\left(\frac{3}{2}K_0' - 1\right)(1-X)\right] \tag{3}$$

where $X = (V/V_0)^{1/3}$. This equation can be linearized by defining the function $H \equiv PX^2/[3(1-X)]$ so that

$$\ln H = \ln K_0 + \tfrac{3}{2}(K_0' - 1)(1-X). \tag{4}$$

In a fit of $\ln H$ versus $(1-X)$, the intercept is given by $\ln K_0$ and the slope is related to K_0'. A plot of $\ln H$ versus $(1-X)$ is shown in figure 4. The line shown in figure 4 is an error-weighted linear least-squares fit to the data. The propagated error in $\ln H$ was used to estimate the weights. With this EOS, we obtain a bulk modulus of 51.9 ± 1.9 GPa with $K_0' = 4.9 \pm 0.5$. These values agree very well with the EOS parameters extracted using the third-order Birch–Murnaghan EOS.

The resultant pressure–volume EOSs for CaS, together with all of the available high-pressure data, are summarized in figure 2. The full line corresponds to the fitted third-order Birch–Murnaghan EOS and is indistinguishable from the fitted universal EOS. The broken line in the figure represents the second-order Birch–Murnaghan EOS.

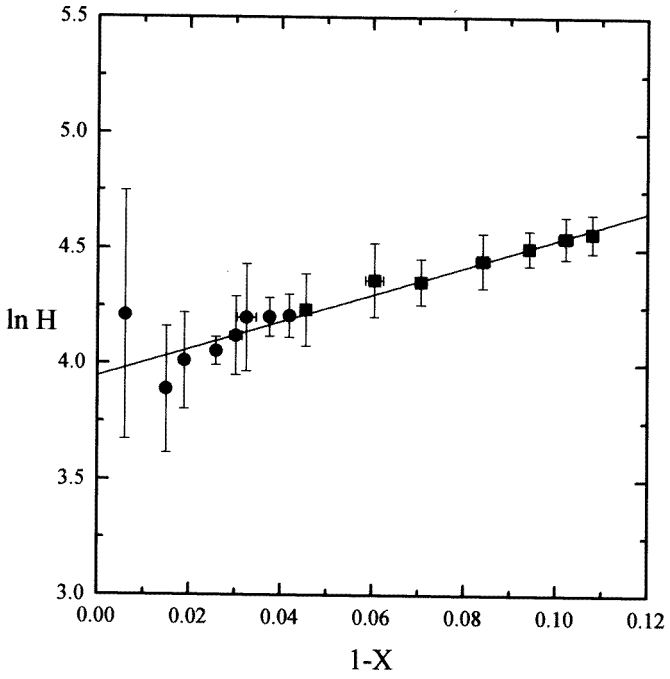

Figure 4. A $\ln H$ versus $(1 - X)$ representation of the CaS compression data. Symbols are the same as those used in figure 3. The full line shows the least-squares fit to the universal EOS.

3. Theory

3.1. An overview of ionic breathing electron-gas models

Theoretical electron-gas descriptions of crystal energetics based on the Gordon–Kim *ansatz* have been remarkably successful in predicting the phase stability, equations of state and thermoelastic properties of a broad class of closed shell halide and oxide systems. In the general Gordon–Kim description, the total crystal charge density is constructed from a superposition of closed shell ions, typically either from Hartree–Fock or from Kohn–Sham calculations. The crystal atomic interaction result from long-range Coulomb and short-range overlap terms. The overlap interactions include contributions from Coulomb, kinetic energy and exchange-correlation terms which are estimated from density functional theory using the local density approximation (LDA).

The most reliable of the Gordon–Kim-based crystal schemes incorporates a spherical deformation, or 'breathing', of the component ion charge densities due to the influence of the crystal environment. The total crystal energy is thus augmented by a self-energy term which is the difference between the ground state energy of the deformed ion and that of the free ion state. Three of the more commonly used electron-gas models which allow spherical charge deformation are the potential-induced breathing (PIB) [9, 10, 14], variationally induced breathing (VIB) [11, 16] and self-consistent ion breathing (SCIB) models [12, 13, 30].

In the PIB and VIB models the crystal-state potential is mimicked by the Watson-sphere potential [18], namely the potential given by a simple charged sphere. The charge on the sphere is typically chosen as the negative of the formal charge of the ion. The PIB and VIB

models are distinguished by the way in which the radius of the Watson shell is determined. In the PIB model, the radius is fixed by matching the potential inside the sphere to the point-ion Coulomb site potential of the crystal. In the VIB model, the Watson-sphere radius is adjusted to minimize the total crystal energy for a given structural configuration.

In the more elaborate SCIB model, the effective crystal potential is not constrained to a Watson-sphere form but is a self-consistent spherically averaged crystal potential. Thus, the effective crystal potential experienced by the ion is a local potential which depends both on the ion's charge density and on the charge density of its environment. In addition to the usual Coulomb and exchange-correlation terms, the potential includes a kinetic energy overlap contribution which is estimated using the Thomas–Fermi local kinetic energy functional. The specific procedure used to construct the spherically averaged site potential is closely related to the procedure described by Edwardson [13] and Johnson *et al* [12]. Once the SCIB site potential has been obtained, it is incorporated as an external potential into the Kohn–Sham [32] atomic calculation and the procedure is continued through self-consistent iteration.

3.2. Formal and numerical details

Using the PIB, VIB and SCIB procedures we have calculated the EOSs and phase stabilities of MgS and CaS at 300 K. In all three of these models, the component ion charge densities were obtained from Kohn–Sham atomic calculations [32] using the Hedin–Lundqvist [33] exchange-correlation functional. The S^{2-} anions were allowed to deform spherically by incorporating either the Watson-sphere or the SCIB external potential in the atomic calculation. The cation charge densities were held rigid to their free-ion states. Test calculations revealed that the cation breathing provides no discernible effect on the calculated properties.

For a given structural configuration, the total crystal static energy, $\Phi_0(V)$, includes the Madelung energy (calculated using the Ewald method [34]) the self-energy (or distortion energy) and the short-ranged overlap interaction energy. The self-energy of the S^{2-} ion was given as the difference between the ground state energy of the deformed ion and that of an arbitrary fixed reference S^{2-} state. The overlap interactions, which include Coulomb, kinetic energy, exchange and correlation contributions, were calculated in the pair approximation using a modified Gordon–Kim-like scheme (described below). The Coulomb contribution to the overlap interaction is computed exactly whereas the LDA is used to estimate the kinetic energy and exchange-correlation terms. The short-ranged pair interactions were summed over the direct lattice until convergence to one part in 10^6 in the crystal energy had been achieved.

In the original Gordon–Kim scheme [8], the kinetic energy contributions to the overlap interaction of two atomic charge densities, n_1 and n_2, is given by

$$\Delta T[n_1, n_2] = T_0[n_1 + n_2] - T_0[n_1] - T_0[n_2] \tag{5}$$

where

$$T_0[n_i] = \tfrac{3}{10}(3\pi^2)^{2/3} \int \mathrm{d}\boldsymbol{r}\, n_i(\boldsymbol{r})^{5/3} \tag{6}$$

is the Thomas–Fermi local density estimate for the total kinetic energy of the charge distribution $n_i(\boldsymbol{r})$. Subsequent work by Waldman and Gordon [35] stressed that, since the local Thomas–Fermi approximation underestimates the kinetic energy relative to the Kohn–Sham or Hartree–Fock calculations, the overlap contribution should be scaled in order to be more consistent with the self-energy atomic calculations. In this regard, rather than using

the static scale factors employed by Waldman and Gordon, we introduce non-empirical dynamic scale factors to adjust our estimates of the overlap kinetic energy contribution. In this procedure, the kinetic energy contribution to the short-ranged overlap energy is given by

$$\Delta T[n_1, n_2] = \frac{3}{10}(3\pi)^{2/3} \int \mathrm{d}\boldsymbol{r}\left[\gamma_{12}(n_1 + n_2)^{5/3} - \gamma_1 n_1^{5/3} - \gamma_1 n_1^{5/3}\right] \tag{7}$$

Here

$$\gamma_i = T_{KS}[n_i]/T_{TF}[n_i] \tag{8}$$

is the ratio of the Kohn–Sham and Thomas–Fermi kinetic energies of atom i and

$$\gamma_{12} = (n_1\gamma_1 + n_2\gamma_2)/(n_1 + n_2). \tag{9}$$

This density-weighed interpolation formula for γ_{12} was first suggested by Rae [36], but in the context of the estimation of exchange interaction energies.

In our calculations, the exchange and correlation contribution to the overlap energy is given by the unscaled Gordon–Kim expression:

$$\Delta E_{xc}[n_1, n_2] = E_{xc}[n_1 + n_2] - E_{xc}[n_1] - E_{xc}[n_2]. \tag{10}$$

For the E_{xc} local density functional we use the Hedin–Lundqvist form [33]. It should be stressed that scale factors are not required for the exchange overlap contribution since the same exchange-correlation energy expression is used in the Kohn–Sham atomic calculations.

In order to compare the theoretical EOS calculations with the room temperature experimental data, we included the thermal contribution to the calculated crystal free energy *via* quasi-harmonic lattice dynamics. At 300 K, this thermal correction is small and is not expected to vary significantly among the various electron-gas models. Therefore, we used the volume-dependent thermal free energy calculated for the VIB model as an estimate of the thermal correction for the PIB and SCIB models as well.

In the quasi-harmonic approximation, the thermal contribution to the Helmholtz free energy of a crystal at a temperature, T, and volume, V, is given by

$$A_{th}(T, V) = \sum_i \frac{h\nu_i}{2} + kT\ln(1 - \mathrm{e}^{-h\nu_i/(kT)}) \tag{11}$$

where h is Plank's constant, k is Boltzmann's constant and the summation is over all vibrational modes, ν_i, in the Brillouin zone. The ν_i were obtained throughout the Brillouin zone by diagonalization of the VIB dynamical matrix. The lattice dynamical matrix element expressions for the VIB model were recently derived by Chizmeshya *et al* [16]. Sufficient convergence of the thermal contribution was achieved using 5178 and 10 542 points in the first Brillouin zones of the B1 and B2 lattices, respectively.

To obtain the theoretical EOSs for the B1, B2, B3 and B4 lattices, we calculated the total crystal Helmholtz free energy, $A(T, V) = \Phi_0(V) + A_{th}(T, V)$, as a function of volume along a 300 K isotherm. To extract the equation of state parameters, the calculated $A(V)$ isotherm points were fitted to the third-order Birch–Murnaghan expressed for the crystal free energy, namely

$$A(V) = A_0 + \frac{3}{2}V_0K_0\left[\frac{3}{4}(1 + 2\xi)\left(\frac{V_0}{V}\right)^{4/3} - \frac{1}{2}\xi\left(\frac{V_0}{V}\right)^2 - \frac{3}{2}(1 + \xi)\left(\frac{V_0}{V}\right)^{2/3} + \frac{1}{2}\left(\frac{3}{2} + \xi\right)\right] \tag{12}$$

where $\xi \equiv \frac{3}{4}(4 - K_0')$ and A_0 is the zero-pressure free energy at 300 K.

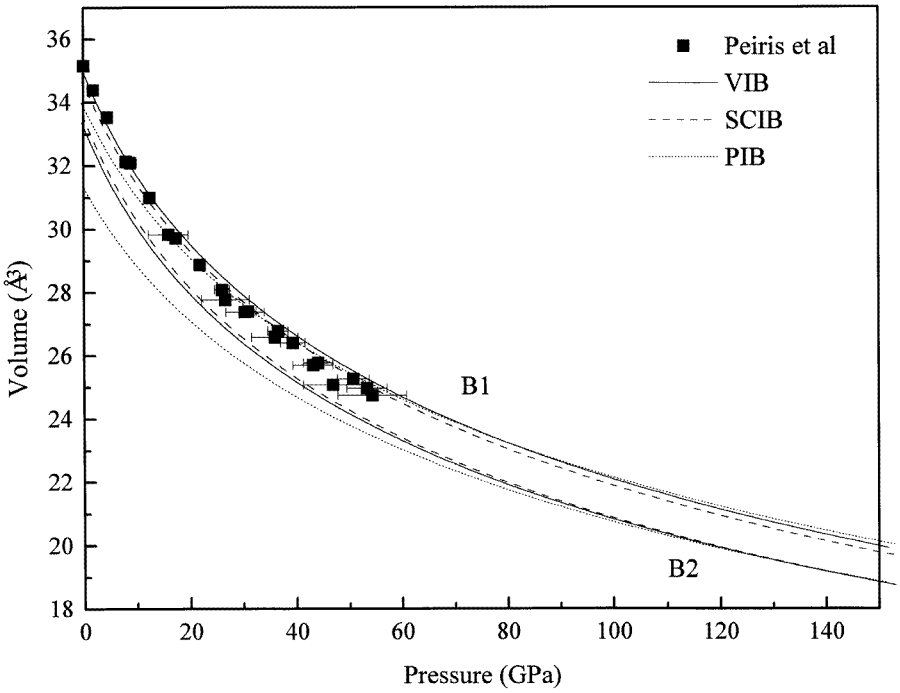

Figure 5. Calculated 300 K EOSs of the B1 and B2 phases of MgS using the VIB, SCIB and PIB electron-gas models. Compression data of the B1 phase from Peiris *et al* [17] are shown for comparison.

3.3. Numerical results and discussion

Figures 5 and 6 compare the experimental EOSs of MgS [17] and CaS [42] (and this study) with those calculated from VIB, SCIB and PIB electron-gas models. Summaries of the calculated and experimental EOS parameters of MgS and CaS are listed in table 2.

In general, all three of the electron-gas models give a reasonably good representation of the EOSs for these binary alkaline-earth sulphides. The differences among the models are relatively small, especially at high pressures. Most striking is the similarity in the theoretical equations of state for the VIB and SCIB models. This similarity is also found in the calculated high-pressure EOS of the B2 phase. The greatest disparity among the models is found in the calculated properties near ambient pressure. For the VIB model, the ambient pressure volumes for MgS and CaS underestimate the experimental values by 0.6% and 2.2%, respectively. For SCIB, the calculated volumes are 1.5% and 2.5% too low. The largest discrepancy is found in the PIB model which underestimates the volumes by 3.6% for MgS and 5.3% for CaS. Using first-principles pseudo-potential calculations, Froyen *et al* [37] obtained very similar results to ours in the case of MgS, underestimating the ambient pressure volume by 2.6% at 300 K. This comparison was made by adding to their calculated static lattice volume the VIB thermal expansion correction at 300 K.

Although the calculated EOSs are in good agreement with the high-pressure data, all of the theoretical models underestimate the compressibility of these sulphides near ambient pressure. However, the best agreement with data is again found for the VIB model whereas the largest discrepancy is found for the PIB model. The experimentally derived bulk modulus

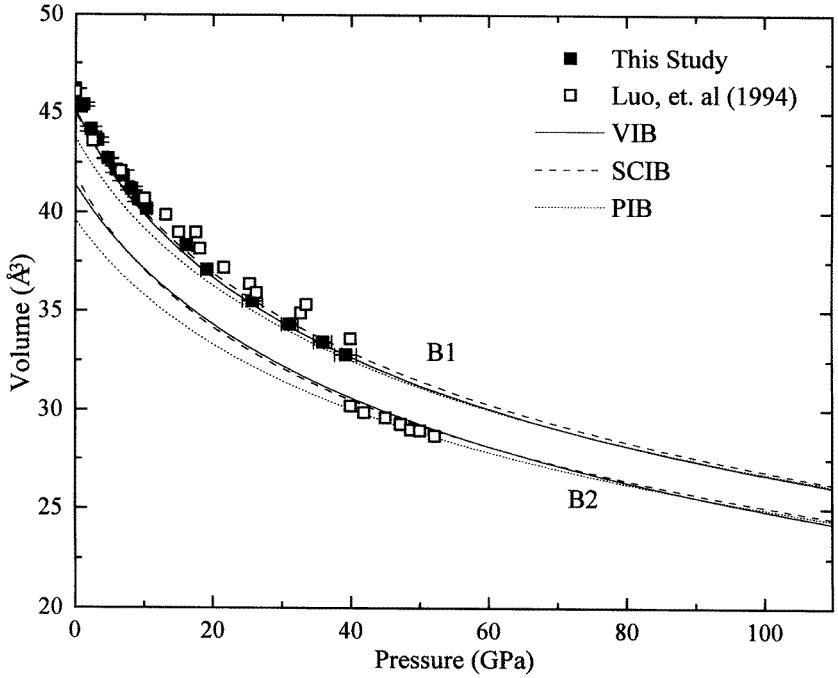

Figure 6. Calculated 300 K EOSs of the B1 and B2 phases of CaS using the VIB, SCIB and PIB electron-gas models. Compression data of the B1 phase from this study (filled squares) and both of the B1 phase and of the B2 phase from the study by Luo *et al* (open squares) are also shown. The calculated EOSs of the B2 phase display good correlation with the measured values.

of MgS is in the range 76.0–81.4 GPa. The VIB and SCIB models give values of 84.1 and 85.5 GPa, respectively, for the bulk modulus of MgS, whereas the PIB model predicts a value of 95.8 GPa. In comparison, Froyen *et al* [37] obtained a value of 82 GPa for the bulk modulus of MgS from their first-principles pseudo-potential calculation (without thermal correction). For CaS, the experimentally derived bulk modulus is in the range 51.9–64 GPa. The VIB and SCIB models again show the best agreement with experiment, with calculated values of 62.3 and 67.8 GPa respectively whereas the PIB model overestimates the value of the bulk modulus of CaS and gives a value of 72.7 GPa.

All three electron-gas models correctly predict that the B1 phase for MgS and CaS is more stable than is the B2 (caesium chloride structure) phase at ambient pressure. The predicted B1–B2 transition pressures for the various theoretical models are listed in table 2. It is interesting that the VIB and PIB models give nearly the same values for the transition pressure, even though these two models were the most disparate. The SCIB model, on the other hand, predicts the transition pressure to be quite high for both compounds. For MgS, the B1–B2 transition has not yet been observed. However, in the case of CaS, Luo *et al* [42] reported this transition to occur near 40 GPa. This value is in good agreement with the predictions both from the VIB (42 GPa) and from the PIB (44 GPa) models.

Syassen [31] has pointed out, in several of his studies, that there is a systematic trend in the values of the transition pressure of the alkaline-earth chalcogenides, which can be related to the cation–anion radius ratio. In figure 7, we present a plot of this relationship for the observed B1–B2 transition pressures and the ion radius ratios of the alkaline-earth

Table 2. Calculated and experimental properties of the B1 phases of MgS and CaS and the predicted B1–B2 phase transition pressure.

	V_0 (Å^3)	K_0 (GPa)	K_0'	B1–B2 P_t (GPa)	$\Delta V/V_t$ (%)
MgS (B1)					
Experimental					
Peiris *et al* (third-order B–M)	35.170	79.8 ± 3.7	3.71 ± 0.34		
Peiris *et al* (second-order B–M)		76.0 ± 1.3	4.0		
Peiris *et al* (universal)		81.4 ± 2.9	3.57 ± 0.32		
Theory					
VIB	34.95	84.1	4.11	105	−5.7
SCIB	34.63	85.5	4.05	>200	
PIB	33.88	95.8	4.19	103	−5.8
CaS (B1)					
Experimental					
This study (third-order B–M)	46.19 ± 0.02	52.6 ± 1.4	4.6 ± 0.2		
This study (second-order B–M)		56.3 ± 0.6	4.0		
This study (universal)		52.4 ± 1.0	4.9 ± 0.2		
Luo *et al*	46.03	64	4.2	40	−10.2
Theory					
VIB	45.12	62.3	4.20	42	−6.1
SCIB	44.96	67.8	4.06	120	−6.6
PIB	43.70	72.7	4.15	44	−7.7

B–M, Birch–Murnaghan.

chalcogenides. The transition pressure of CaS [42] is shown to be consistent with this trend. Also shown in figure 7 are the transition pressures of MgO and MgS extrapolated from the existing data. The transition pressures for MgS obtained using the VIB and PIB models are 105 and 103 GPa, respectively. These values are significantly lower than the value of 228 GPa inferred from the empirical scaling. However, this extrapolation of the transition pressure from the experimental trend in figure 7 may not be reliable since the phase transformation in the magnesium chalcogenide system has not yet been reported.

The SCIB model predicts the B1 phase to be more stable than the B2 phase up to 120 GPa for CaS and 200 GPa for MgS. However, we find that the absolute energy difference between the two phases at ambient pressure is larger in SCIB than it is in VIB in spite of their very similar EOSs. A detailed analysis of the energetics in the two models suggests that the origin of this difference resides in the self-energies of the S^{2-} ions in the B1 and B2 lattices. Further investigations of this point are being performed.

We also investigated the relative stability of the B3 (zinc blende) and B4 (wurtzite) structure both for MgS and for CaS using the VIB model. Mittendorf *et al* [38] found that the B4 phase of MgS can be epitaxially stabilized in thin films on aluminium substrates. Stability calculations using the VIB model predict that, at ambient pressure, the B1 phase of MgS is only slightly more stable than both the B4 wurtzite phase and the B3 zinc blende phase. In particular, the wurtzite and zinc blende phases are respectively 0.009 and 0.019 au higher in free energy than is the B1 MgS phase at zero pressure and 300 K. The small energy differences among these phases at ambient pressure are certainly consistent with the observation of epitaxial stabilization of the wurtzite MgS phase. In fact, under tension, the wurtzite phase becomes more stable than the B1 phase below a pressure of only −6.9 GPa. Similarly, the VIB calculations predict the B1–B4 phase transition in CaS

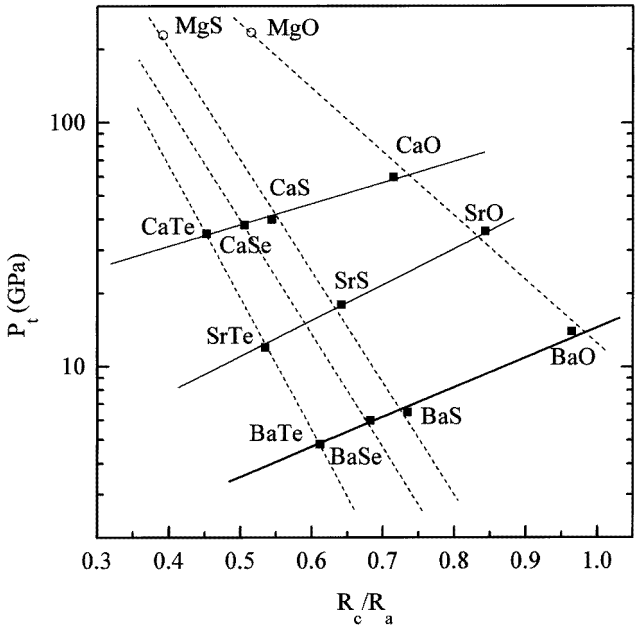

Figure 7. A systematic representation of the log of the B1–B2 transition pressure for the alkaline-earth chalcogenides as a function of their cation–anion radius ratio. This figure is an adaptation of a similar plot by Syassen [31]. Open circles for MgS and MgO represent predicted transition pressures based on these systematic trends. The experimental transition pressure for BaO used here is the pressure at which the low-pressure tetragonal phase of BaO transforms to a distorted B2 structure [39].

to be at −6.1 GPa. At zero pressure the VIB free energies of the B4 and B3 phases are, respectively, 0.012 and 0.029 au higher than the B1 phase.

Comparison can also be made between the observed and calculated volumes of the wurtzite (B4) MgS phase. Mittendorf *et al* [38] measured a value of 43.2 Å^3 for the volume of the epitaxially stabilized B4 phase. The VIB model predicts that the 300 K volume of the B4 phase at ambient pressure is 40.9 Å^3. Under hydrostatic tension, the calculated volume of the B4 phase is 50.4 Å^3 at the B1–B4 transition pressure. Although first-principles calculations have not yet been performed for the B4 MgS phase, Froyen *et al* [37] obtain a value of 44.2 Å^3 (including the VIB thermal correction) for the 300 K ambient volume of the B3 phase using the pseudo-potential method. This value is also in good agreement with the VIB model which predicts a volume of 43.69 Å^3 for the B3 MgS phase under ambient conditions. At this point, no experimental data are available for the B4 phase of CaS, but, according to the VIB calculation, the volume of the B4 phase at ambient pressure is 53.0 Å^3, whereas the volume at the B1–B4 transition pressure is 61.8 Å^3.

4. Conclusions

The level of agreement between the VIB calculated results and the experimental equations of state of these sulphides is generally similar to that found for the alkaline-earth oxides as well as for a number of other oxide phases. Both VIB and SCIB models show very similar results in predicting equations of state and elastic properties of the two materials. The

equations of state calculated by the PIB model, on the other hand, predict both compounds to be less compressible in B1 and B2 phases, in comparison to the other two models. However, in predicting the phase stability of these compounds, the VIB and PIB models are in good agreement, whereas this result obtained from the SCIB model predicts the B1 phases of MgS and CaS to be stable up to much higher pressure.

The best overall results for the VIB model are found when the kinetic energy interaction term is scaled in the density-weighted scheme described above. If the kinetic energy interaction term is not scaled, as in the usual Gordon–Kim scheme, the volume of the B1 phase is further reduced, by about 5%, for all three electron-gas models studied here. This was also borne out in our earlier calculations concerning MgO and CaO [16]. With the scaling procedure described above, we find a comparable accuracy in the oxide B1 equations of state to that which we find here for the sulphide phases.

Finally, a suite of scaled VIB calculations was performed in order to examine the phase stabilities of MgS and CaS in the wurtzite (B4) and zinc blende (B3) structures. Our calculations show that the B1 phases of MgS and CaS transform to the wurtzite structure under tension, whereas the zinc blende phase is found to have a higher energy than either the B1 or the B4 phase. For MgS, this is consistent with the results of an experimental study conducted by Mittendorf *et al* [38], who observed a bi-axially strained B4 phase of MgS on an aluminium substrate. Our calculated ambient pressure volume for this phase is in good agreement with the observed value as well.

Acknowledgments

The authors gratefully acknowledge the assistance of Jingzhu Hu and Mary VerHelst-Voorhees during collection of the x-ray data. David Mao provided synchrotron beam time at the Brookhaven National Light Source for the diffraction experiments. Beam line X17C is funded by the National Science Foundation under the Earth Sciences Facilities and Instrumentation Programme. This work was funded in part by NSF under the ASU Materials Research Group grant DMR-9121570. Andrew Chizmeshya was supported through the EG&G Idaho long-term research initiative under DOE Idaho Operations Office contract DE-AC07-761DO1570.

References

[1] Bukowinski M S T 1980 *J. Geophys. Res.* **85** 285
[2] Bukowinski M S T and Hauser J 1980 *Geophys. Res. Lett.* **7** 689
[3] Bukovwinski M S T 1982 *J. Geophys. Res.* **87** 303
[4] Aidun J, Bukowinski M S T and Ross M 1984 *Phys. Rev.* B **29** 2611
[5] Wei S-H and Krakauer H 1985 *Phys. Rev. Lett.* **55** 1200
[6] Christensen N E and Satpathy S 1985 *Phys. Rev. Lett.* **55** 600
[7] Mehl M J, Cohen R E and Krakauer H 1988 *J. Geophys. Res.* **93** 8009
[8] Gordon R G and Kim Y S 1972 *J. Chem. Phys.* **56** 3122
[9] Mehl M J, Hemley R J and Boyer L L 1986 *Phys. Rev.* B **33** 8685
[10] Cohen R E, Boyer L L and Mehl M J 1987 *Phys. Rev.* B **35** 5749
[11] Wolf G H and Bukowinski M S T 1988 *Phys. Chem. Miner.* **15** 209
[12] Johnson M D, Subbaswamy K R and Senatore G 1987 *Phys. Rev.* B **36** 9202
[13] Edwardson P J 1989 *Phys. Rev. Lett.* **63** 55
[14] Isaak D G, Cohen R E and Mehl M J 1990 *J. Geophys. Res.* **95** 7055
[15] Zhang H and Bukowinski M S T 1996 *Phys. Rev.* B submitted
[16] Chizmeshya A, Zimmermann F M, LaViolette R A and Wolf G H 1994 *Phys. Rev.* B **50** 15 559
[17] Peiris S M, Campbell A J and Heinz D L 1994 *J. Phys. Chem Solids* **55** 413

[18] Watson R E 1958 *Phys. Rev.* **111** 1108
[19] Mao H-K, Xu J and Bell P M 1986 *J. Geophys. Rev.* **91** 4673
[20] Finger L W, Hazen R M, Zhou G, Mao H-K and Bell P M 1981 *Appl. Phys. Lett.* **39** 892
[21] Zou G, Mao H-K and Bell P M 1982 *Carnegie Institution Washington Yearbook* **81** 392
[22] Peterson O G, Batchelder D N and Simmons R O 1966 *Phys. Rev.* **150** 703
[23] Xu J, Mao H-K and Bell P M 1984 *High. Temp.–High Pressures* **16** 495
[24] Ross M, Mao H-K, Bell P M and Xu J A 1986 *J. Chem. Phys.* **85** 1028
[25] Birch F 1986 *J. Geophys. Res.* **91** 4949
[26] Schlosser H and Ferrante J 1988 *Phys. Rev.* B **37** 4351
[27] Perez-Albuerne E A and Drickamer H G 1965 *J. Chem. Phys.* **43** 1381
[28] Bridgman P W 1940 *Proc. Am. Acad. Arts Sci.* **74** 21
[29] Richet P, Mao H-K and Bell P M 1988 *J. Geophys. Res.* **93** 15 279
[30] LeSar R 1983 *Phys. Rev.* B **28** 6812
[31] Syassen K 1985 *Phys. Status Solidi* **91** 11
[32] Kohn W and Sham L J 1965 *Phys. Rev.* **140** 1133
[33] Hedin L and Lundqvist B I 1971 *J. Phys. C: Solid State Phys.* **4** 2064
[34] Ewald P P 1921 *Ann. Phys., Lpz* **64** 253
[35] Waldman M and Gordon R G 1979 *J. Chem. Phys.* **71** 1325
[36] Rae A I M 1975 *Mol. Phys.* **29** 467
[37] Froyen S, Wei S-H and Zunger A 1988 *Phys. Rev.* B **38** 10 125
[38] Mittendorf H 1965 *Z. Phys.* **183** 113
[39] Weir S T, Yohra Y K and Ruoff A L 1986 *Phys. Rev.* B **33** 4221
[40] Heinz D L and Jeanloz R 1984 *J. Appl. Phys.* **55** 885
[41] Vinet P, Ferrante J, Smith J R and Rose J H 1986 *J. Phys. C: Solid State Phys.* **19** L467
[42] Luo H, Greene R G, Ghandehari K, Li T and Ruoff A L 1994 *Phys. Rev.* B **50** 16 232